104 (2025) 104978

Contents lists available at ScienceDirect

Poultry Science

journal homepage: www.elsevier.com/locate/psj

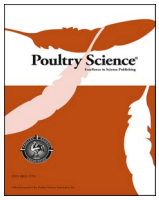

Full-Length Article

Hexavalent chromium induces ferroptosis in small intestinal tissue of broilers through GPX4/HMGB1/p38-MAPK pathway

Juezhang Wang, Bingtong Fan, Weina Liu, Zibo Ma, Ruiqin Guo, Jinhang Guo, Jinglu Wang, Ding Zhang, Zilong Sun, Ci Liu *

College of Veterinary Medicine, Shanxi Agricultural University, Taigu, Jinzhong, 030801, PR China

ARTICLE INFO

Keywords:
Hexavalent chromium
Ferroptosis
p38-MAPK
Small intestine
Broiler

ABSTRACT

As a major environmental heavy metal pollutant, hexavalent chromium (**Cr(VI)**) causes irreversible damage to animals and humans. Nevertheless, how Cr(VI) exposure causes intestinal damage in broilers remains inadequately explored. This study explores Cr(VI)-induced poisoning using potassium dichromate to build a Cr(VI) poisoning model. The results indicate that Cr(VI) exposure evidently reduced the body weight and the functions of liver and kidney in broilers. Histopathological analysis revealed different degrees of structural damage in all three segments of the small intestines by Cr(VI) exposure. Moreover, Cr(VI) exposure downregulated ZO-1, Occludin, and Claudin-1, while altering the diversity of cecal microbiota to impair the intestinal barrier function. Additionally, with increasing Cr(VI) concentration, the contents of Fe^{2+}, ROS, and LPO in all three intestinal segments showed a dose-dependent increase. The levels of GPX4, SLC7A11, FTL, and FTH1 were downregulated by Cr(VI), while the levels of p38-MAPK, phosphorylated p38, TFR1, and HMGB1 were upregulated. This study suggests that Cr(VI)-induced ROS can trigger ferroptosis through the GPX4/HMGB1/p38-MAPK pathway, leading to intestinal barrier dysfunction and ultimately reducing the production performance of broilers. This provides foundation of theory for understanding the effects of Cr(VI) exposure on the small intestine.

Introduction

Cr(VI) is a proven toxin and mutagen commonly used in light and heavy industries (Bagchi et al., 2002; Iyer et al., 2023). Studies have reported that Cr(VI) pollution caused by the rapid development of industry is still serious and widespread, involving a wide range of areas, such as air, soil and water resources (Gupta et al., 2024; Kazakis et al., 2017). Currently, several national governments have promulgated the compulsory rules to limit Cr(VI) (Hedberg et al., 2020), and Cr(VI) has been recognized as a Class I carcinogen by IARC (Zhou et, al.2018). Released Cr(VI) accumulates in the environment, and it poses serious risks to human health and food safety throughout the food chain (Lee et al., 2019). Cr(VI) enters cells through nonspecific phosphate/sulfate anionic transporters and is reduced to Cr(III) by antioxidants such as glutathione (Jomova et al., 2011). The produced Cr(III) is generally considered to have no toxic effects (Kamila et al., 2023), but this process depletes antioxidant enzymes, further leading to excessive generation of ROS (Marchi et al., 2023). The accumulated ROS triggers LPO and various forms of cell death (Wang et al., 2023).

Ferroptosis is a specific death pattern and is different from other cell death modalities owing to its dependence on iron and LPO (Dixon et al., 2012). Intracellular Fe^{2+} accumulation, GPX4 inactivation, and LPO accumulation are key characteristics of ferroptosis (Li et al., 2020). The Fe^{3+} concentrations in the physiological state are in dynamic equilibrium. In the bloodstream, Fe^{3+} forms a complex with transferrin and enters cells via the TFR1. Once inside, it is reduced to Fe^{2+} and stored in the LIP or exported out of the cell by ferroportin. Excess Fe^{2+} induces the Fenton reaction to produce hydroxyl radicals that react with polyunsaturated fatty acids to induce LPO, eventually triggering ferroptosis (Jiang et al., 2021). Moreover, excessive ROS depletes GPX4 and accelerates PUFA oxidation, leading to ferroptosis (Kakade et al., 2020; Li et al., 2021). During ferroptosis, HMGB1 is released (Wen et al., 2019). After HMGB1 binds to the receptor for RAGE, the MAPK pathway can be activated (Sappington et al., 2002; Yang et al., 2020). Specifically, the p38-MAPK pathway upregulates TFR1, thus increasing intracellular Fe^{3+} levels and promoting ferroptosis (Wang et al., 2023). Current studies indicate that heavy metals could induce ferroptosis via different pathways. For example, Cd inhibits the GPX4 pathway by producing

* Corresponding author.
E-mail address: liuci1988@163.com (C. Liu).

https://doi.org/10.1016/j.psj.2025.104978
Received 6 December 2024; Accepted 2 March 2025
Available online 3 March 2025

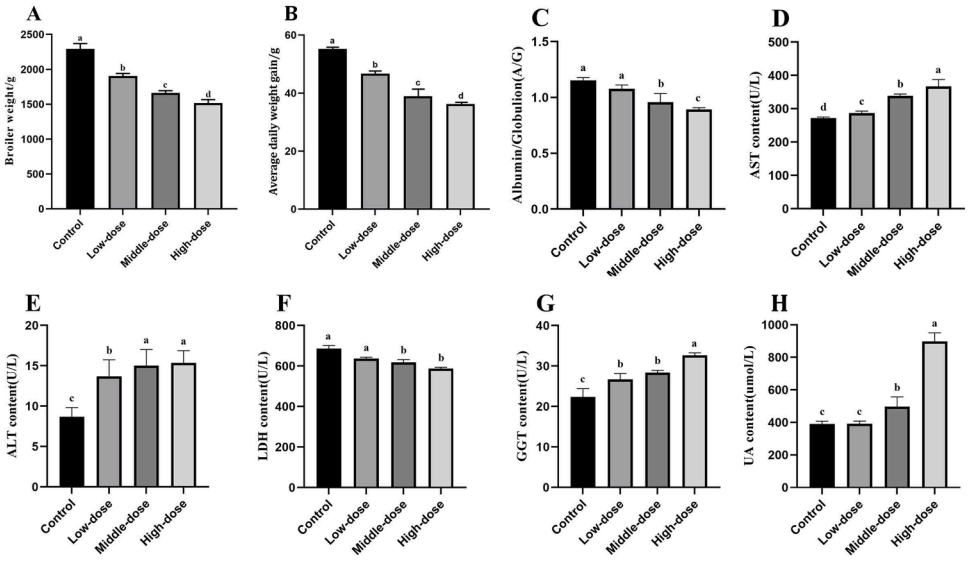

Fig. 1. Results of Cr (VI) on physical signs and serum biochemical parameters of broilers. (A) indicates the final body weight of broilers; (B) indicates the average daily weight gain of broilers; (C) indicates the A/G; (D) represents the content of AST; (E) represents the content of ALT; (F) indicates the content of LDH; (G) indicates the content of GGT; (H) indicates the content of UA.

ROS to induce ferroptosis in the mouse hippocampus (Wang et al., 2024). Similarly, another study has reported that Cd can cause ferroptosis in the mouse kidney by upregulating HMGB1 expression (Qiu et al., 2023). Additionally, excess Fe activates the p38 pathway, regulating ferroptosis in osteoblasts (Zhao et al., 2021). These studies highlight that ferroptosis is a key mechanism in heavy-metal-induced toxicity.

The global demand for affordable animal protein is increasing. Based on the USDA, global broiler yield reached 102.389 million tons in 2023. Broilers raised on farms in the vicinity of chemical factories are at risk of exposure to Cr(VI) through drinking, feeding, and inhalation. Therefore, investigating the damage by Cr(VI) in broilers is of practical importance. Exposure to environmental Cr(VI) for a long term can cause intestinal damage, negatively impacting the growth performance of broilers. Consequently, exploring the mechanisms of intestinal injury caused by Cr(VI) is essential for improving production performance.

Materials and methods

Animal experiment

In this study, one-day-old Ross 308 broilers of similar weights and backgrounds were used. To establish a model of Cr(VI)-induced small intestinal damage, 100 broilers were randomly assigned to four groups: control, low-, middle-, and high-dose groups. Broilers were raised in Experimental Animal Management Center of Shanxi Agricultural University where could provide appropriate temperature and light exposure to ensure the smooth progression of the experiments. The environmental temperature remained at 32 °C in the first week, decreased by 2 °C every week, and finally remained at 22 °C. Each group of broilers is provided with sufficient drinking water and an equal amount of feed daily. During the experiment, the feed was provided by Zhengda Company (Hebei, China). At 7 d, the broilers of low-, middle-, and high-dose groups were gavaged with $K_2Cr_2O_7$ (Xiya Reagent, Shandong, China) solution for 35 d, with Cr(VI) concentrations of 0.0104 g/kg·BW, 0.0156 g/kg·BW, and 0.0312 g/kg·BW, and the control group were gavaged same volume of physiological saline. The weight and diet of the broilers were recorded daily and adjust the dosage of $K_2Cr_2O_7$ based on weight. After the final gavage, the broilers were in abrosia for 12 h and weighed to determine their final weight.

On day 42, all the broilers were euthanized. Blood and cecal contents were collected. After the complete removal of small intestine tissue from broilers, the U-shaped intestinal segment connected to the muscular stomach is the duodenum, the short and straight intestinal segment connected to the cecum is the ileum, and the remaining intestinal segments are the jejunum. When collecting samples, try to gather 4cm in the central part of each intestinal segment, as much as possible to ensure consistency in the experiment. Subsequently, a portion of the small intestine tissue with 4 % paraformaldehyde fixed, while the other tissues and cecal contents were stored in a −80°C freezer for further analysis. The experimental protocol adhered to the China Animal Protection Commission's requirements and was ratified by the Shanxi Agricultural University Animal Care and Use Commission.

Serum testing

Venous blood samples were collected into the blood tubes, saved at 25°C for 40 min, and centrifuged at 4,000 r·min^{-1} to separate the serum. Then collected the serum, and biochemical parameters including A/G, AST, ALT, LDH, GGT, and UA were measured using an automated biochemical analyzer (Biostar V7, Seamaty Technology Co, Chengdu, China).

Detection of oxidation in small intestinal

At −80°C, the small intestinal tissue was removed and homogenized. Using commercial assay kits and measured the absorbance (optical density (OD)) with a microplate reader (Synergy LX, Agilent, Santa Clara, California, USA) to determine the levels of Fe^{2+} (Jiancheng Bioengineering Institute, Nanjing, China), ROS (Beyotime, Shanghai, China), and LPO (Michy Biomedical Technology Co, Suzhou, China) in different segments of the broilers' small intestines.

Histopathological examination

The samples of small intestine were removed from a 4 % paraformaldehyde solution and make the tissue samples into paraffin for HE staining. The tissue sections were observed using Nikon Eclipse E100 microscope (Nikon Co., Tokyo, Japan) to observe histopathological changes. ImageJ (Version 1.38) was used to quantify alterations in the intestinal villi and crypts.

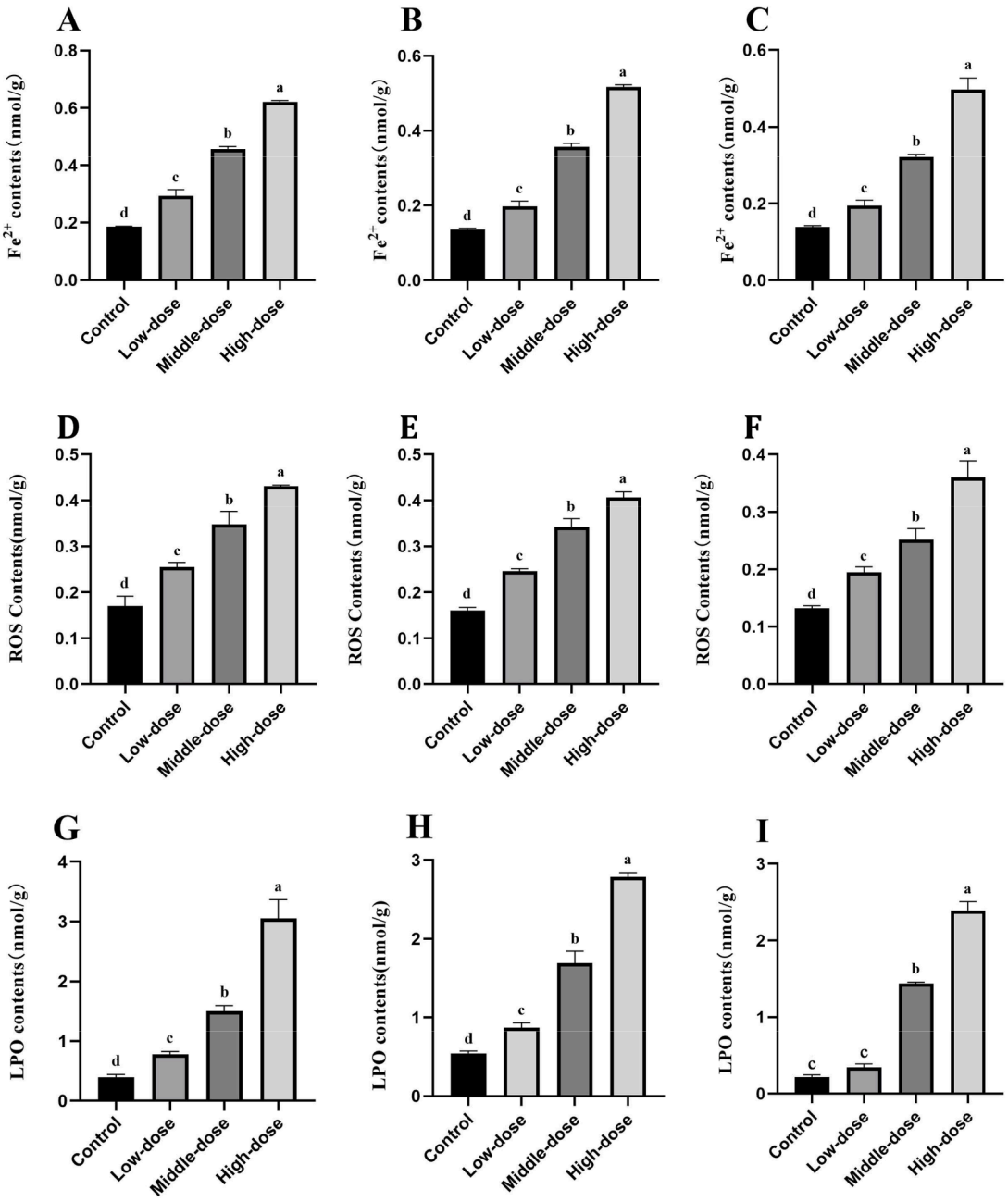

Fig. 2. Effects of Cr (VI) on Fe $^{2+}$, ROS, and LPO in small intestinal tissues. (A-C) respectively indicate the contents of Fe $^{2+}$ in duodenum, jejunum, and ileum; (D-F) respectively indicate the contents of ROS in duodenum, jejunum, and ileum; (G-I) respectively indicate the content of LPO in duodenum, jejunum, and ileum.

Real-time fluorescence quantitative PCR (qPCR)

The small intestine was homogenized on ice, extracted total RNA using TRIzol. Reverse transcription of RNA using the reverse transcription kit (Tolo Bio, Shanghai, China). Subsequently, cDNA was diluted and analyzed via quantitative polymerase chain reaction (qPCR) (Bio-Rad, Hercules, California, USA). **Supplementary table** shows the primers for the target genes used in the qPCR.

Western blotting

The small intestine tissue was ground into powder and extracted the total protein. After separating protein by electrophoresis, transferring protein to a PVDF membrane. Then blocked the membrane for two hours. After PVDF membrane was washed, submersed the membrane in primary antibody at 4 °C for 14 h. The antibodies used included β-actin (1:3,000; Abmart, Shanghai, China), ATPase (1:5,000; Abmart), ZO-1 (1:2,000; ABclonal, Wuhan, China), Occludin (1:700, ABclonal), Claudin-1 (1:600, Abmart) GPX4 (1:2,000; Abmart), SLC7A11 (1:1,800; Abmart), FTL (1:3,000; Abmart), FTH1 (1:2100; Abmart,), p38 (1:1,300, Abmart), p-p38 (1:600; Wanleibio, Shenyang, China), HMGB1 (1:600, Abmart), and TFR1 (1:1,000, Abmart). The PVDF membrane was washed and submersed in a secondary antibody for one hour at 25 °C. The goat anti-mouse (1:15,000, Bioss, Beijing, China) was used for β-actin, ATPase and HMGB1. The goat anti-rabbit (1:8,000, Bioss) was used for ZO-1, Occludin, Claudin-1, GPX4, SLC7A11, FTL, FTH1, p38, p-p38 and TFR1. An enhanced chemiluminescence Plus kit (Biosharp, Hefei, China) was used to treat the PVDF membrane and photographed. Subsequently, used ImageJ software (version 1.38) for quantitative analysis of proteins.

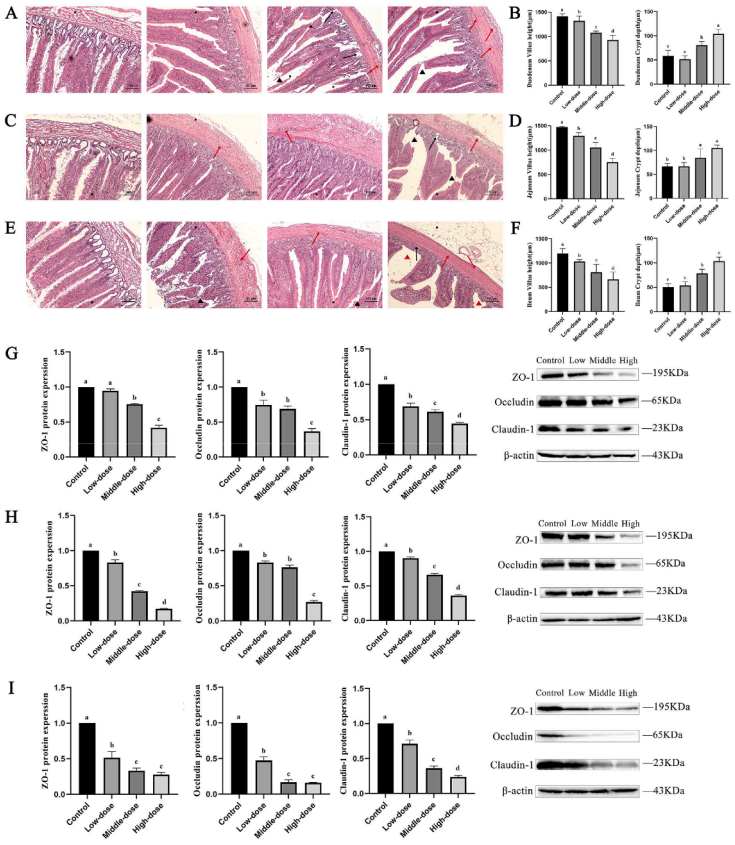

Fig. 3. Results of histopathological changes induced by Cr (VI). (A, C, E) indicate the histopathological observation of the control, low-, middle-, and high-dose groups in duodenum, jejunum, and ileum. Black and red triangles in the picture represent the rupture and loss of intestinal villi, the black and red arrows represent the loss of crypts and inflammatory cell infiltration; (B, D, F) indicate the height of the villus and the depth of the crypts of the duodenum, jejunum, and ileum; (G-I) respectively indicate the protein expressions and the depth of the electrophoresis band by Western blotting for ZO-1, Occludin and Claudin-1 in the duodenum, jejunum and ileum.

16S-rDNA microbiome analysis

Abstracted DNA from the cecal contents and tested thereafter. Clean data were obtained following amplification, purification, and on-machine sequencing. After denoising, amplicon sequence variants (**ASVs**) were used to create an operational taxonomic unit (**OTU**) table. The ASV features and sequences were gained, followed by diversity and difference of species analyses.

Data assessment

All data were expressed as mean ± standard deviation. GraphPad Prism8 software and IBM SPSS Statistics 25 software were used for data processing and graphing. The One-way ANOVA was used to assess the data and Tukey's test was used for post hoc multiplicity testing. The significance was represented by $p < 0.05$. The differences between groups in the figures were represented by different lowercase letters.

Results

Physical signs and serum biochemical parameters

To indicate the influence of Cr(VI) on the broiler's physical indices, the weight of every group was measured. Results show a significant drop in final body weight and average daily weight gain with increasing Cr (VI) concentration ($p < 0.05$) (Fig. 1**A and B**). Serum biochemical analysis revealed the metabolic dysfunction caused by Cr(VI). In comparison with the control group, the A/G and LDH levels were lower in the Cr(VI) exposure groups ($p < 0.05$). Conversely, AST, ALT, GGT, and UA contents increased ($p < 0.05$) (Fig. 1**C–H**). These changes were most pronounced in the high-dose group.

Fe^{2+} and oxidative damage in small intestinal tissues

In the duodenum and jejunum (Fig. 2), in comparison with the control group, the contents of Fe^{2+}, ROS, and LPO in the low-, middle-, and high-dose groups were increased ($p < 0.05$). In the ileum, in addition to LPO in the low-dose group, the content of Fe^{2+}, ROS, and LPO in the low-, middle-, and high-dose groups were above than control group, with the highest increase observed in the high-dose group ($p < 0.05$).

Histopathological changes

Fig. 3**(A–F)** shows the histopathological observations of sections of small intestinal tissues. The small intestine villi and the crypt structures are arranged tightly and neatly in the control groups of duodenum, jejunum, and ileum. In the middle- and high-dose groups of the duodenum, inflammatory cell infiltration, villus rupture, and crypt structural loss were observed. In the low-, middle- and high-dose groups of the jejunum and ileum, with Cr(VI) concentration increased, the damage of villi and crypt structures was progressively increased. By evaluating the villus height and crypt depth, the results revealed that with an increase in the Cr(VI) concentration, the height of villi in small intestinal tissues gradually shortens compared with that in the control group ($p < 0.05$). Compared with the control group, the depth of crypts in the middle- and high-dose groups of duodenum, jejunum, and ileum significantly increased ($p < 0.05$).

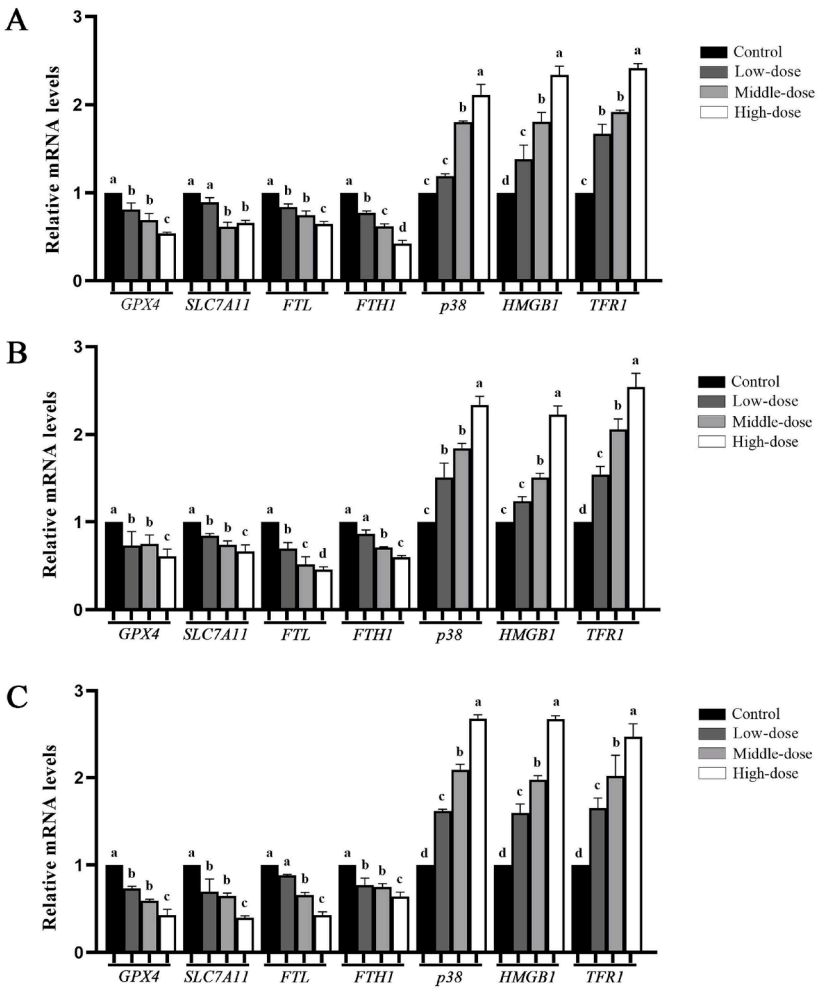

Fig. 4. Effects of Cr (VI) on the mRNA expressions of GPX4/HMGB1/p38-MAPK in the small intestinal tissues. (A) indicates the mRNA expressions in the duodenum; (B) indicates the mRNA expressions in the jejunum; (C) indicates the mRNA expressions in the ileum.

Tight junction protein expressions in small intestinal tissues

Fig. 3**(G–I)** illustrates the level of tight junction (TJ) proteins expression in the small intestines. In the duodenum, except ZO-1 in the low-dose group, the expression of ZO-1, Occludin, and Claudin-1 protein in the Cr(VI) treatment groups was downregulated compared with that in the control group in a dose-dependent manner ($p < 0.05$). In the jejunum and ileum, the expression of these TJ proteins in the low-, middle- and high-dose groups was downregulated compared with that in the control group ($p < 0.05$). Additionally, the levels of proteins expression from the high-dose group were peaked in the intestinal tissues.

mRNA expression in small intestinal tissues

The mRNA expression of the GPX4/HMGB1/p38-MAPK pathway in small intestinal tissues is shown in Fig. 4. Obviously distinct with the control group, the mRNA expression of *GPX4, SLC7A11, FTL*, and *FTH1* in the middle- and high-dose groups decreased, while *p38, HMGB1*, and *TFR1* mRNA levels increased in different segments of the small intestine ($p < 0.05$). In the duodenum, by comparison to the control group, the mRNA levels of *GPX4, FTL*, and *FTH1* in the low-dose group were downregulated, while *HMGB1* and *TFR1* mRNA levels were upregulated ($p < 0.05$). In the jejunum, in contrast with the control group, the mRNA levels of *GPX4, SLC7A11*, and *FTL* in the low-dose group were downregulated, while *p38* and *TFR1* mRNA levels were upregulated ($p < 0.05$). In the ileum, by comparison to the control group, the mRNA levels of *GPX4, SLC7A11*, and *FTH1* in the low-dose group were downregulated, while *p38, HMGB1*, and *TFR1* mRNA levels were upregulated ($p < 0.05$). Overall, the mRNA expressions of *p38, HMGB1*, and *TFR1* exhibited positive dose-dependent relationship with Cr(VI) concentration, whereas the mRNA expressions of *GPX4, SLC7A11, FTL*, and *FTH1* exhibited negative dose-dependent relationship.

Ferroptosis protein expressions in small intestinal tissues

The protein expression of ferroptosis is shown in Fig. 5. In different segments of the small intestine, in comparison with the control group, the protein expression of GPX4, SLC7A11, FTL, and FTH1 in the middle- and high-dose groups was downregulated ($p < 0.05$), and the change peaked in the high-dose group. In comparison to the control group, the protein expression of GPX4 and SLC7A11 in the low-dose group was downregulated ($p < 0.05$) in the duodenum and ileum; and the protein expression of SLC7A11 and FTH1 in the low-dose group was downregulated ($p < 0.05$) in the jejunum.

HMGB1/p38-MAPK pathway protein expressions in small intestinal tissues

The protein expression of HMGB1/p38-MAPK pathway in the small intestinal tissues is shown in Fig. 6. In the duodenum and jejunum, the protein expressions of p38, p-p38, HMGB1, and TFR1 in the Cr(VI)

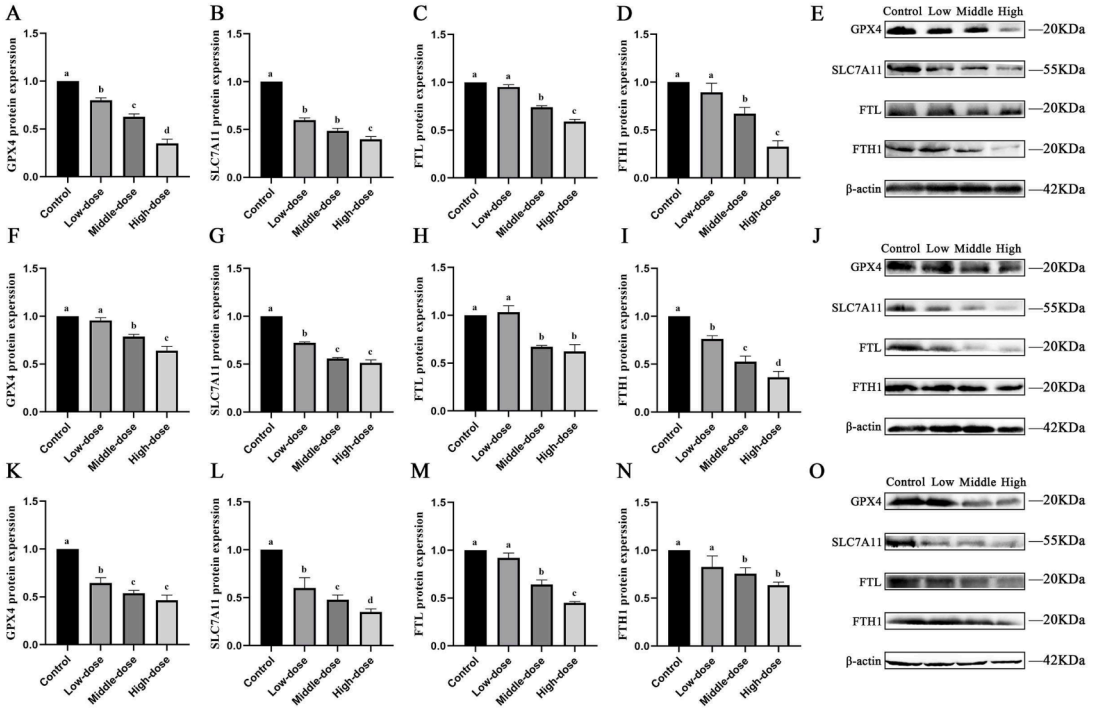

Fig. 5. Effects of Cr (VI) on the protein expressions of ferroptosis. (A-E) indicate the protein expressions and the depth of the electrophoresis band in the duodenum; (F-J) indicate the protein expressions and the depth of the electrophoresis band in the jejunum; (K-O) indicate the protein expressions and the depth of the electrophoresis band in the ileum.

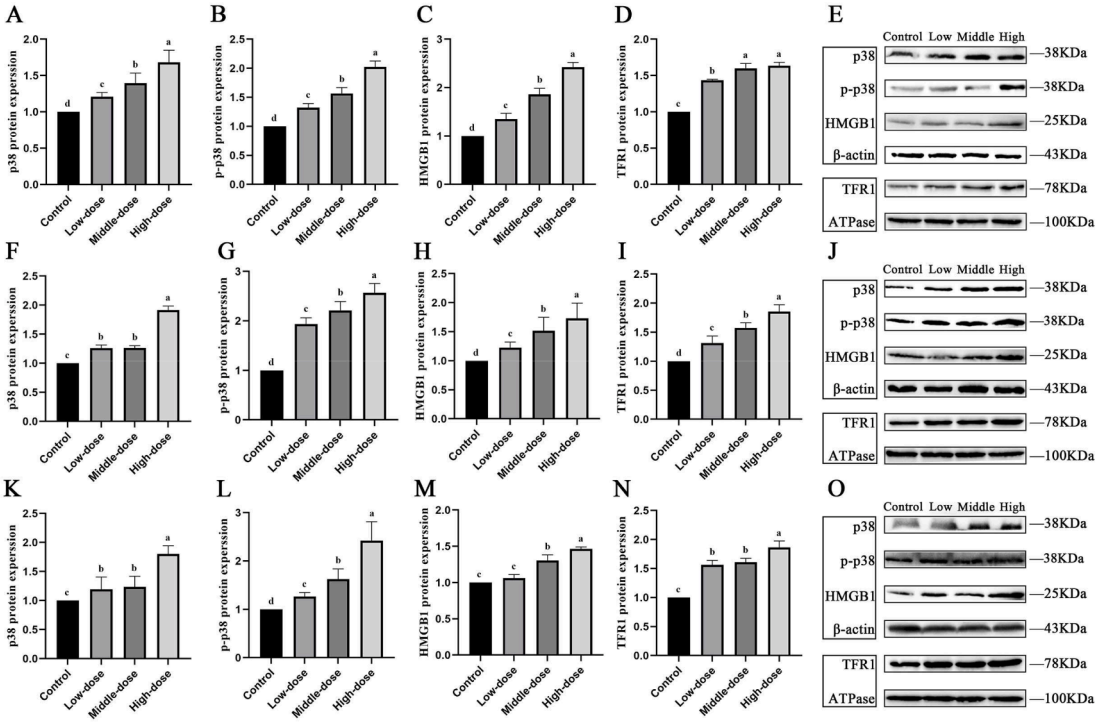

Fig. 6. Effects of Cr (VI) on the protein expressions of HMGB1/p38-MAPK. (A-E) indicate the protein expressions and the depth of the electrophoresis band in the duodenum; (F-J) indicate the protein expressions and the depth of the electrophoresis band in the jejunum; (K-O) indicate the protein expressions and the depth of the electrophoresis band in the ileum.

exposure groups were upregulated ($p < 0.05$). In the ileum, by comparison with the control group, the expressions of p38, p-p38, and TFR1 in the Cr(VI) exposure groups were upregulated, the HMGB1 expression in the middle- and high-dose groups was raised ($p < 0.05$).

Gut microbiota ***analysis***

The number of ASVs possessed by microbiota species of cecal contents in different groups was reflected in the sample ASVs Venn diagram

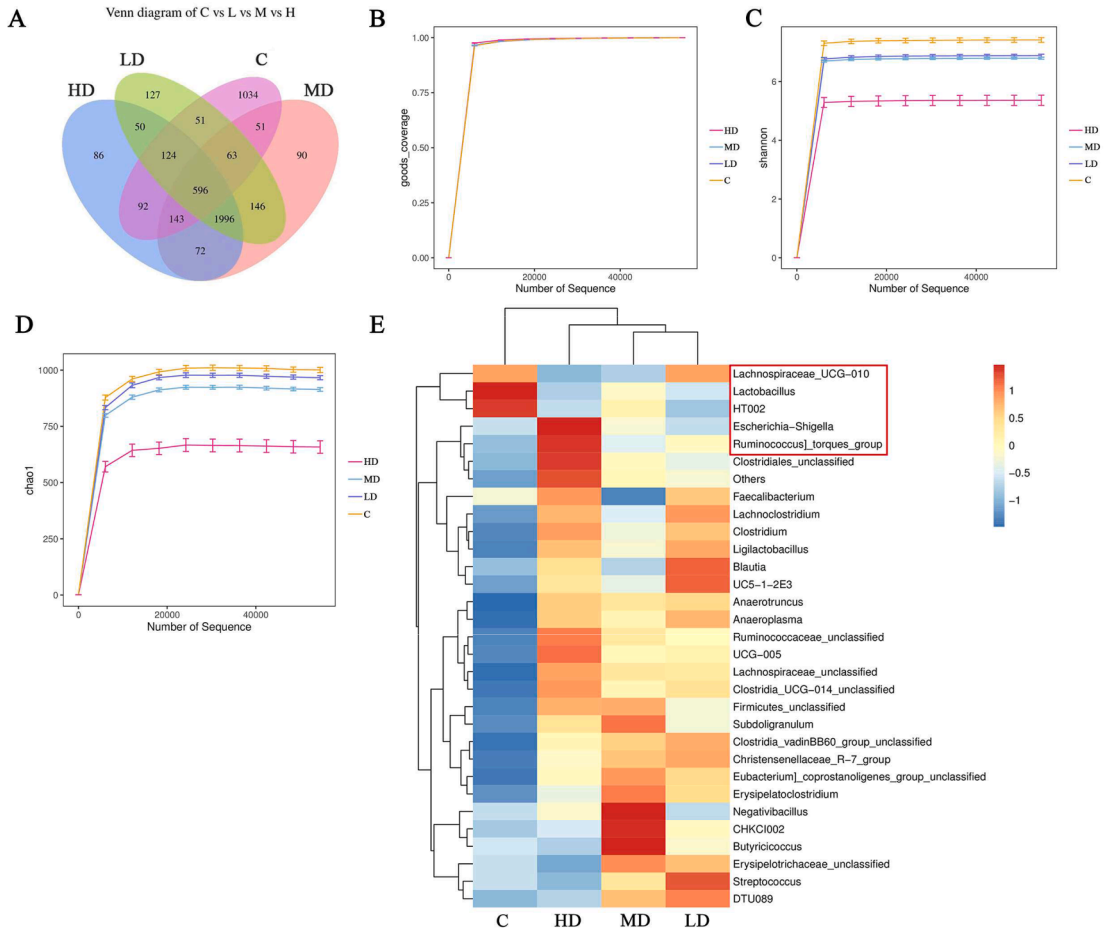

Fig. 7. Results of 16S-rDNA microbiome analysis. (A) Venn diagram shows number of unique and shared ASV (at 13 % similarity) among intestinal microbial under different groups; (B-D) Alpha-diversity of the intestinal microbial communities include goods-coverage, Shannon and Chao1 indexes among four groups; (E) Heatmap. Each row represents the species, each column represents the grouping, and the blue-to-red gradient color is used to reflect the change in abundance from low to high, the closer to blue, the lower the abundance, the closer to red, the higher the abundance.

(Fig. 7**A**). Totals of 4,721 ASVs were tested, with 596 ASVs common in all groups. The unique ASV count for the control group (C), low-dose group (LD), middle-dose group (MD), and high-dose group (HD) were 1034, 127, 90, and 86, respectively. The α-diversity of microbiota was examined in all groups. The goods-coverage values were approximately one, indicating that all the samples were almost complete. Microbial community diversity and richness were shown using the Chao 1 and Shannon indices (Fig. 7**B–D**). The results show that as the exposure concentration of Cr(VI) increased, microbial community diversity and richness in the broilers gradually decreased. Fig. 7**E** reflects the species abundance at the genus level. Compared to the control group, the *Lachnospiraceae_UCG_010, Lactobacillus*, and *HT002*, were significantly downregulated by Cr(VI). Conversely, the *Escherichia, Shigella*, and *Ruminococcus torques*, significantly increased, disrupting the intestinal microbiota barrier of the broilers.

Discussion

Cr(VI) pollution has become a serious environmental concern owing to human activities. When Cr(VI) enters the environment, it disrupts animal metabolism and significantly affects human health (Li et al., 2023). Accumulating evidence suggests that Cr(VI) causes multi-organ damage when absorbed into the body (Bakshi et al., 2018; Singh et al., 2022). The intestine, an organ crucial for nutrient absorption, is closely associated with poultry performance. Cr(VI) inevitably damages the intestine during absorption and metabolism (El Cafsi et al., 2020; Xing et al., 2022; Mu et al., 2023). This study explored the mechanism of Cr(VI) in small intestinal injury in broilers, confirming that Cr(VI) exposure reduced broiler growth capability and impaired metabolic function. Nutrient absorption by the intestinal epithelium is related to crypt depth and villus length. Increasing evidence suggests that exposure to heavy metals can shorten intestinal villi and increase crypt depth, ultimately compromising health (Xie et al., 2020; Tian et al., 2023). In this paper, Cr(VI) exposure shortened villi length and increased the crypt depth in each group of broilers, indicating reduced intestinal absorption capacity and mucosal function. These findings suggest that Cr (VI) exposure impairs nutrient absorption, leading to reduced growth performance in broilers.

In addition to absorption and digestion, the intestinal tract acts as an innate barrier that maintains intestinal homeostasis and hinders the growth of pathogenic bacteria. The intestinal barrier comprises mechanical, chemical, microbiological, and immune barriers. The TJ is a critical structure that maintains the mechanical barrier between intestinal mucosal epithelial cells and is mainly composed of ZO-1, Occludin, and Claudin-1 (Furuse et al., 1998; Martìn-Padura et al., 1998; Zhang et al., 2019). When the TJ is mutated, reduced, or absent, the permeability of the intestinal epithelial space increases, and harmful substances are more likely to enter systemic circulation through the TJ (Wan et al., 2024). TJ can be damaged due to heavy metal exposure. For example, Jiang et al. confirmed that Cd exposure causes TJ damage and reduces the levels of ZO-1, Occludin, and Claudin-3 in mouse intestinal epithelial cells (Jiang et al., 2020). Liu et al. confirmed that Pb could damage the gut and reduce the levels of ZO-1, ZO-2, Claudin-1, and Occludin (Liu et al., 2024). In this paper, Cr(VI) exposure can

downregulate the expressions of ZO-1, Occludin, and Claudin-1, suggesting that Cr(VI) exposure can damage TJ and increase intestinal permeability, impairing the mechanical barrier function of the small intestine in broilers. Current studies have indicated that heavy metal exposure adversely affects the gut microbial barrier, and that imbalance in the gut microbiome increases gut and organ damage (Yao et al., 2019; Zhong et al., 2021). *Lachnospiraceae_UCG_010* was positively correlated with the intestinal biobarrier function of broilers (Kan et al., 2021), Dempsey et al. confirmed that most *Lactobacillus* species are beneficial bacteria (Dempsey et al., 2022), and Xu et al. confirmed that *HT002* is abundant as a beneficial bacterium after probiotic administration (Xu et al., 2024). In this paper, Cr(VI) exposure decreased the richness of *Lachnospiraceae_UCG_010, Lactobacillus*, and *HT002*, while increasing the richness of *Escherichia-Shigella* and *Ruminococcus torques*. These confirm that Cr (VI) exposure can impair the microbial barrier function. Damage of the mechanical and microbial barriers compromises intestinal integrity, facilitating entry of Cr(VI) into the systemic circulation and leading to damage in other organs.

To clarify whether exposure to Cr(VI) induces ferroptosis, the classic biochemical indicators of ferroptosis (ROS, Fe^{2+}, and LPO) were measured in the small intestinal tissues, with results showing that these levels increased after Cr(VI) exposure. Moreover, SLC7A11/GPX4 axis is a defense mechanism against ferroptosis. SLC7A11 is a regulatory factor of ferroptosis. The downregulation of SLC7A11 leads to a reduction in the activity of GPX4, leading to the accumulation of LPO and triggering ferroptosis (Koppula et al., 2021). Current research indicates that heavy metals can induce ferroptosis by inhibiting the SLC7A11/GPX4 pathway, such as Cu(II) amplifies ferroptosis by promoting autophagic degradation of GPX4 (Xue et al., 2023); Cd can induce ferroptosis by inhibiting SLC7A11-GSH-GPX4 axis (Hong et al., 2022). In this study, the expressions of SLC7A11 and GPX4 were significantly downregulated following Cr(VI) exposure, indicating Cr(VI) induces ferroptosis in the small intestinal tissues of broilers through the SLC7A11/GPX4 axis. HMGB1, released after ferroptosis, has been reported to further promote ferroptosis by binding to RAGE and activating the MAPK pathway (Chen et al., 2022). This activation upregulated the expression of TFR1, resulting in an increase in intracellular Fe^{2+} and an imbalance in iron homeostasis (Yu et al., 2015). Fe^{2+} homeostasis is regulated by FTL and FTH1 (Mancias et al., 2014). FTH1 converts Fe^{2+} to Fe^{3+} and combines with FTL to reduce the toxicity of Fe^{2+}, impeding ferroptosis. To further elucidate the pathway of Cr(VI)-induced ferroptosis in the small intestine, the expressions of HMGB1, p38, TFR1, FTH1, and FTL were measured in this study. Cr(VI) upregulated the expressions of HMGB1, p38, p-p38, and TFR1, while downregulating the expressions of FTH1 and FTL. These indicate that Cr(VI) exposure can activate the HMGB1/p38-MAPK pathway to disrupt iron homeostasis, exacerbate the accumulation of Fe^{2+}, and further induce ferroptosis in the small intestinal tissues of broilers.

Overall, this study revealed that Cr(VI) triggering ferroptosis via the GPX4/HMGB1/p38-MAPK pathway leads to damage to the small intestinal tissues of broilers in a dose dependent manner. Therefore, ferroptosis is implicated in Cr(VI)-induced enterotoxicity, which disrupts the intestinal barrier and tissue structure, leading to intestinal malabsorption and reducing broiler production. This study offers a new visual angle into the influence of Cr(VI) in broiler intestines, contributing to the development of strategies to improve broiler growth performance.

Declaration of competing interest

The authors declared that there is no conflict of interest to this study.

Acknowledgments

Funding: The National Natural Science Foundation of China (31802248), the Fundamental Research Program of Shanxi Province (Grant No. 202203021211265 and 202203021222180), and the Introducing Talents and Doctoral Research of Shanxi Agricultural University (2017YJ08).

Supplementary materials

Supplementary material associated with this article can be found, in the online version, at doi:10.1016/j.psj.2025.104978.

References

Bagchi, D., Stohs, S.J., Downs, B.W., Bagchi, M., Preuss, H.G., 2002. Cytotoxicity and oxidative mechanisms of different forms of chromium. Toxicology 180, 5–22. https://doi.org/10.1016/S0300-483X(02)00378-5.

Bakshi, A., Panigrahi, A.K., 2018. A comprehensive review on chromium induced alterations in fresh water fishes. Toxicol Rep 5, 440–447. https://doi.org/10.1016/j.toxrep.2018.03.007.

Chen, R., Kang, R., Tang, D., 2022. The mechanism of HMGB1 secretion and release. Exp. Mol. Med. 54, 91–102. https://doi.org/10.1038/s12276-022-00736-w.

Dempsey, E., Corr, S.C., 2022. Lactobacillus spp. For Gastrointestinal Health: current and Future perspectives. Front. Immunol. 13, 840245. https://doi.org/10.3389/fimmu.2022.840245.

Dixon, S.J., Lemberg, K.M., Lamprecht, M.R., Skouta, R., Zaitsev, E.M., Gleason, C.E., Patel, D.N., Bauer, A.J., Cantley, A.M., Yang, W.S., Morrison, B., Stockwell, B.R., 2012. Ferroptosis: an iron-dependent form of nonapoptotic cell death. Cell 149, 1060–1072. https://doi.org/10.1016/j.cell.2012.03.042.

El Cafsi, I., Bjeoui, S., Rabeh, I., Nechi, S., Chelbi, E., El Cafsi, M., Ghram, A., 2020. Effects of ochratoxin A on membrane phospholipids of the intestine of broiler chickens, practical consequences. Animal 14, 933–941. https://doi.org/10.1017/S1751731119002593.

Furuse, M., Fujita, K., Hiiragi, T., Fujimoto, K., Tsukita, S., 1998. Claudin-1 and -2: novel integral membrane proteins localizing at tight junctions with no sequence similarity to occluding. J. Cell Biol. 141, 1539–1550. https://doi.org/10.1083/jcb.141.7.1539.

Gupta, P.K., Nair, V.K., Dalvi, V., Dhali, S., Malik, A., Pant, K.K., 2024. Field-scale assessment of soil, water, plant, and soil microbiome in and around Rania-Khan Chandpur Chromium contaminated site, India. J. Hazard. Mater. 467, 133747. https://doi.org/10.1016/j.jhazmat.2024.133747.

Hedberg, Y.S., Wei, Z., Moncada, F., 2020. Release of hexavalent chromium from cement collected in Honduras and Sweden. Contact Dermatitis 83, 122–124. https://doi.org/10.1111/cod.13508.

Hong, H., Lin, X., Xu, Y., Tong, T., Zhang, J., He, H., Yang, L., Lu, Y., Zhou, Z., 2022. Cadmium induces ferroptosis mediated inflammation by activating Gpx4/ager/p65 axis in pancreatic β-cells. Sci. Total Environ. 849, 157819. https://doi.org/10.1016/j.scitotenv.2022.157819.

Iyer, M., Anand, U., Thiruvenkataswamy, S., Babu, H.W.S., Narayanasamy, A., Prajapati, V.K., Tiwari, C.K., Gopalakrishnan, A.V., Bontempi, E., Sonne, C., Barceló, D., Vellingiri, B., 2023. A review of chromium (Cr) epigenetic toxicity and health hazards. Sci. Total Environ. 882, 163483. https://doi.org/10.1016/j.scitotenv.2023.163483.

Jiang, X., Stockwell, B.R., Conrad, M., 2021. Ferroptosis: mechanisms, biology and role in disease. Nat. Rev. Mol. Cell Biol. 22, 266–282. https://doi.org/10.1038/s41580-020-00324-8.

Jiang, Z., Mu, W., Yang, Y., Sun, M., Liu, Y., Gao, Z., Li, J., Gu, P., Wang, H., Lu, Y., Ba, Q., Wang, H., 2020. Cadmium exacerbates dextran sulfate sodium-induced chronic colitis and impairs intestinal barrier. Sci. Total Environ. 744, 140844. https://doi.org/10.1016/j.scitotenv.2020.140844.

Jomova, K., Valko, M., 2011. Advances in metal-induced oxidative stress and human disease. Toxicology 283, 65–87. https://doi.org/10.1016/j.tox.2011.03.001.

Kakade, A., Salama, E.S., Pengya, F., Liu, P., Li, X., 2020. Long-term exposure of high concentration heavy metals induced toxicity, fatality, and gut microbial dysbiosis in common carp, Cyprinus carpio. Environ. Pollut. 266, 115293. https://doi.org/10.1016/j.envpol.2020.115293.

Kamila, S., Shaw, P., Islam, S., Chattopadhyay, A., 2023. Ecotoxicology of hexavalent chromium in fish: an updated review. Sci. Total Environ. 890, 164395. https://doi.org/10.1016/j.scitotenv.2023.164395.

Kan, L., Guo, F., Liu, Y., Pham, V.H., Guo, Y., Wang, Z., 2021. Probiotics Bacillus licheniformis improves intestinal health of subclinical necrotic enteritis-challenged broilers. Front. Microbiol. 12, 623739. https://doi.org/10.3389/fmicb.2021.623739.

Kazakis, N., Kantiranis, N., Kalaitzidou, K., Kaprara, E., Mitrakas, M., Frei, R., Vargemezis, G., Tsourlos, P., Zouboulis, A., Filippidis, A., 2017. Origin of hexavalent chromium in groundwater: the example of Sarigkiol Basin, Northern Greece. Sci. Total Environ. 593-594, 552–566. https://doi.org/10.1016/j.scitotenv.2017.03.128.

Koppula, P., Zhuang, L., Gan, B., 2021. Cystine transporter SLC7A11/xCT in cancer: ferroptosis, nutrient dependency, and cancer therapy. Protein Cell 12, 599–620. https://doi.org/10.1007/s13238-020-00789-5.

Lee, C.P., Hsu, P.Y., Su, C.C., 2019. Increased prevalence of Sjogren's syndrome in where soils contain high levels of chromium. Sci. Total Environ. 657, 1121–1126. https://doi.org/10.1016/j.scitotenv.2018.12.122.

Li, A., Ding, J., Shen, T., Han, Z., Zhang, J., Abadeen, Z.U., Kulyar, M.F., Wang, X., Li, K., 2021. Environmental hexavalent chromium exposure induces gut microbial dysbiosis in chickens. Ecotoxicol. Environ. Saf. 227, 112871. https://doi.org/10.1016/j.ecoenv.2021.112871.

Li, J., Cao, F., Yin, H.L., Huang, Z.J., Lin, Z.T., Mao, N., Sun, B., Wang, G., 2020. Ferroptosis: past, present and future. Cell. Death. Dis. 11, 88. https://doi.org/10.1038/s41419-020-2298-2.

Li, T., Lv, Y., Wu, Z., Guo, M., Liu, R., Zeng, W., Zheng, Y., 2023. Systematic assessment of hexavalent chromium-induced damage to male fertility and the preventive role of melatonin: a longitudinal study from the translational point of view. Mol. Hum. Reprod. 29, gaad020. https://doi.org/10.1093/molehr/gaad020.

Liu, Z.H., Ai, S., Xia, Y., Wang, H.L., 2024. Intestinal toxicity of Pb: structural and functional damages, effects on distal organs and preventive strategies. Sci. Total Environ. 931, 172781. https://doi.org/10.1016/j.scitotenv.2024.172781.

Mancias, J.D., Wang, X., Gygi, S.P., Harper, J.W., Kimmelman, A.C., 2014. Quantitative proteomics identifies NCOA4 as the cargo receptor mediating ferritinophagy. Nature 509, 105–109. https://doi.org/10.1038/nature13148.

Marchi, S., Guilbaud, E., Tait, S.W.G., Yamazaki, T., Galluzzi, L., 2023. Mitochondrial control of inflammation. Nat. Rev. Immunol. 23, 159–173. https://doi.org/10.1038/s41577-022-00760-x.

Martìn-Padura, I., Lostaglio, S., Schneemann, M., Williams, L., Romano, M., Fruscella, P., Panzeri, C., Stoppacciaro, A., Ruco, L., Villa, A., Simmons, D., Dejana, E., 1998. Junctional adhesion molecule, a novel member of the immunoglobulin superfamily that distributes at intercellular junctions and modulates monocyte transmigration. J. Cell Biol. 142, 117–127. https://doi.org/10.1083/jcb.142.1.117.

Mu, J., Guo, Z., Wang, X., Wang, X., Fu, Y., Li, X., Zhu, F., Hu, G., Ma, X., 2023. Seaweed polysaccharide relieves hexavalent chromium-induced gut microbial homeostasis. Front. Microbiol. 13, 1100988. https://doi.org/10.3389/fmicb.2022.1100988.

Qiu, W., Ye, J., Su, Y., Zhang, X., Pang, X., Liao, J., Wang, R., Zhao, C., Zhang, H., Hu, L., Tang, Z., Su, R., 2023. Co-exposure to environmentally relevant concentrations of cadmium and polystyrene nanoplastics induced oxidative stress, ferroptosis and excessive mitophagy in mice kidney. Environ. Pollut. 333, 121947. https://doi.org/10.1016/j.envpol.2023.121947.

Sappington, P.L., Yang, R., Yang, H., Tracey, K.J., Delude, R.L., Fink, M.P., 2002. HMGB1 B box increases the permeability of caco-2 enterocytic monolayers and impairs intestinal barrier function in mice. Gastroenterology 123, 790–802. https://doi.org/10.1053/gast.2002.35391.

Singh, V., Singh, N., Verma, M., Kamal, R., Tiwari, R., Sanjay Chivate, M., Rai, S.N., Kumar, A., Singh, A., Singh, M.P., Vamanu, E., Mishra, V., 2022. Hexavalent-chromium-induced oxidative stress and the protective role of antioxidants against cellular toxicity. Antioxidants (Basel) 11, 2375. https://doi.org/10.3390/antiox11122375.

Tian, X., Lin, X., Zhao, J., Cui, L., Gao, Y., Yu, Y.L., Li, B., Li, Y.F., 2023. Gut as the target tissue of mercury and the extraintestinal effects. Toxicology 484, 153396. https://doi.org/10.1016/j.tox.2022.153396.

Wang, B., Wang, Y., Zhang, J., Hu, C., Jiang, J., Li, Y., Peng, Z., 2023. ROS-induced lipid peroxidation modulates cell death outcome: mechanisms behind apoptosis, autophagy, and ferroptosis. Arch. Toxicol. 97, 1439–1451. https://doi.org/10.1007/s00204-023-03476-6.

Wang, D., Wu, Y., Zhou, X., Liang, C., Ma, Y., Yuan, Q., Wu, Z., Hao, X., Zhu, X., Li, X., Shi, J., Chen, J., Fan, H., 2024. Cadmium exposure induced neuronal ferroptosis and cognitive deficits via the mtROS-ferritinophagy pathway. Environ. Pollut. 349, 123958. https://doi.org/10.1016/j.envpol.2024.123958.

Wan, S., Wang, L., Hao, Z., Zhu, L., Mao, X., Li, H., Sun, P., Yin, W., Fan, K., Zhang, H., Li, B., Nie, W., Li, Z., Sun, N., 2024. Baicalin ameliorates the gut barrier function and intestinal microbiota of broiler chickens. Acta. Biochim. Biophys. Sin. (Shanghai) 56, 634–644. https://doi.org/10.3724/abbs.2024029.

Wang, X., Tan, X., Zhang, J., Wu, J., Shi, H., 2023. The emerging roles of MAPK-AMPK in ferroptosis regulatory network. Cell. Commun. Signal. 21, 200. https://doi.org/10.1186/s12964-023-01170-9.

Wen, Q., Liu, J., Kang, R., Zhou, B., Tang, D., 2019. The release and activity of HMGB1 in ferroptosis. Biochem. Biophys. Res. Commun. 510, 278–283. https://doi.org/10.1016/j.bbrc.2019.01.090.

Xie, S., Jiang, L., Wang, M., Sun, W., Yu, S., Turner, J.R., Yu, Q., 2020. Cadmium ingestion exacerbates Salmonella infection, with a loss of goblet cells through activation of Notch signaling pathways by ROS in the intestine. J. Hazard. Mater. 391, 122262. https://doi.org/10.1016/j.jhazmat.2020.122262.

Xing, C., Yang, F., Lin, Y., Shan, J., Yi, X., Ali, F., Zhu, Y., Wang, C., Zhang, C., Zhuang, Y., Cao, H., Hu, G., 2022. Hexavalent chromium exposure induces intestinal barrier damage via activation of the NF-κb signaling pathway and NLRP3 inflammasome in ducks. Front. Immunol. 13, 952639. https://doi.org/10.3389/fimmu.2022.952639.

Xu, L., Liao, J., Li, X., Zhu, L., Wang, X., Xu, B., Li, L., Ze, X., Sun, H., Li, J., 2024. Exploring the mechanism of probiotics in enhancing the utilization of chemical components (or polyphenols) of grape seed extract. Food Chem. 438, 137982. https://doi.org/10.1016/j.foodchem.2023.137982.

Xue, Q., Yan, D., Chen, X., Li, X., Kang, R., Klionsky, D.J., Kroemer, G., Chen, X., Tang, D., Liu, J., 2023. Copper-dependent autophagic degradation of GPX4 drives ferroptosis. Autophagy 19, 1982–1996. https://doi.org/10.1080/15548627.2023.2165323.

Yang, H., Wang, H., Andersson, U., 2020. Targeting inflammation driven by HMGB1. Front. Immunol. 11, 484. https://doi.org/10.3389/fimmu.2020.00484.

Yao, Q., Yang, H., Wang, X., Wang, H., 2019. Effects of hexavalent chromium on intestinal histology and microbiota in Bufo gargarizans tadpoles. Chemosphere 216, 313–323. https://doi.org/10.1016/j.chemosphere.2018.10.147.

Yu, Y., Xie, Y., Cao, L., Yang, L., Yang, M., Lotze, M.T., Zeh, H.J., Kang, R., Tang, D., 2015. The ferroptosis inducer erastin enhances sensitivity of acute myeloid leukemia cells to chemotherapeutic agents. Mol. Cell. Oncol 2, e1054549. https://doi.org/10.1080/23723556.2015.1054549.

Zhang, W., Liu, H., Liu, C., 2019. Biopharmaceutics classification and intestinal absorption of chikusetsusaponin IVa. Biopharm. Drug Dispos. 40, 276–281. https://doi.org/10.1002/bdd.2200.

Zhao, H., Wang, W., Chen, S., 2021. Iron Overload Downregulates Osteoblast Function via ASK1-p38 Pathway-mediated Ferroptosis, 50. Journal of China Medical University, pp. 530–534. https://dx.link.cnki.net/urlid/21.1227.R.20210525.1116.018.

Zhong, G., Wan, F., Lan, J., Jiang, X., Wu, S., Pan, J., Tang, Z., Hu, L., 2021. Arsenic exposure induces intestinal barrier damage and consequent activation of gut-liver axis leading to inflammation and pyroptosis of liver in ducks. Sci. Total Environ. 788, 147780. https://doi.org/10.1016/j.scitotenv.2021.147780.

Zhou, Y., Zhao, Y., Wu, X., Yin, W., Hou, J., Wang, S., Feng, K., Wang, X., 2018. Adsorption and reduction of hexavalent chromium on magnetic greigite (Fe_3S_4)-CTAB: leading role of Fe(ii) and S(-ii). RSC Adv. 8, 31568–31574. https://doi.org/10.1039/c8ra06534a.